RESEARCH ARTICLE

Electrochemical mechanisms of leakage-current in photovoltaic modules

Michael Kempe[1] | Peter Hacke[1] | Joshua Morse[1] | Jichao Li[2] | Yu-Chen Shen[2] | Katherine Han[2]

[1]National Renewable Energy Laboratory, Golden, CO, 80401, USA

[2]SunPower Corporation, San Jose, CA, 95134, USA

Correspondence
Michael Kempe, National Renewable Energy Laboratory, Golden, CO 80401, USA.
Email: michael.kempe@nrel.gov

Abstract

This paper analyzes the mechanisms and pathways for leakage current flow observed in Si photovoltaic modules subjected to high temperature and humidity and a large voltage bias with respect to ground. The current inside of the frame is in the form of electron motion, but in the glass and polymer, it is in at least a large part attributable to the movement of ions. When the mode of current flow changes from electronic to ionic conduction, electrochemical reactions will take place at the interface. This can include reactions that produce volatile chemical species like H_2, CO_x, and O_2, along with ionic species such as OH^- and H_3O^+. Here, we see evidence of the importance of different charge carriers with different diffusion rates and the influence of electrochemical processes involved. The application of negative voltage to the cell circuit affects the resistivity of glass producing surfaces with poor conductivity but with some increases in the electrochemical potential producing complicated interactions that are important when the voltage is changed. In the polymer, there is the development of a space charge region and a chemical gradient providing two oppositional forces to current flow, which when released create a complicated discharge process. Here, we give a basic understanding of the charge/discharge of PV cells highlighting how the specific mechanisms are important in understanding some of the degradation processes in PV modules. We find that there is evidence of multiple significant charge carrier species with different diffusion time scales. The glass/polymer interface forms a depleted region of higher resistance after prolonged exposure to current. Charge also builds up at the polymer to cell antireflective coating interface and mostly flows to the gridlines to experience electrochemical reactions. These complexities result in non-linear behavior where the apparent resistivities of the different layers change during charge/discharging processes, making the modeling of the current flow extremely difficult.

KEYWORDS
capacitance, corrosion, delamination, leakage current, module, photovoltaic, potential induced degradation (PID)

1 | INTRODUCTION

The system voltage of solar panels drives a leakage current between the solar cells and the grounded metal frames. This results in many different forms of potential induced degradation, including shunting, polarization,[1] delamination, and corrosion. This leakage current can be composed of either electronic or ionic charge carriers.[2,3] The Na^+ ions from the glass, or present initially in the encapsulant, or even the cell surface,[4] drift toward the cell through the encapsulant under the electrical field and can accumulate near the metallization fingers as ionic species, in silicon stacking faults causing PID-shunting, or on the SiO_xN_y surface when the cells are at negative potential.[5,6] With the cells at positive bias (negative ground), metals dissolve and form metal ions, resulting in metal oxidation and corrosion.[7,8] To a lesser degree, current will also flow as electrons, which results in a benign transfer of charge. Under an AC current, the rotation of polarized species can be a significant contribution to charge movement for highly insulating materials, but this is unimportant for DC applications. Ion motion is a significant form of charge transport in insulators, and the current flow in glass is almost exclusively ionic. Similarly, the conduction of charge in polymeric materials is dependent on the nature of the polymer and considered as the movement either of electrons or of ions but is primarily ionic, as in the case of Na^+ in EVA.

The accumulated charge, obtained by integrating the leakage current, has been used to evaluate the impact of potential-induced degradation.[8–12] The leakage current is strongly dependent on temperature,[7,13] humidity,[8] geometry,[14] voltage, and impurities.[15–18] However, the electrochemistry caused by the leakage current is not well understood, and its effects on delamination and corrosion induced by these reactions are not well reported. This work investigates the transient current characteristics of a module to try to understand the mechanisms of charger transfer and accumulation. This aids in our understanding of the location of chemical reactions and their nature. We begin to develop a model for the charge accumulation and relaxation in a photovoltaic module, but because of large transient changes to conductivity and charge transport properties, accurately accounting for all conduction processes was not possible.

2 | EXPERIMENTAL

2.1 | Material conductivity/resistivity measurements

Similar to what is reported elsewhere,[19] volume and surface resistivity measurements were performed in a Keithley 6517A electrometer with an 8008 resistivity fixture surrounded by a copper mesh Faraday cage to reduce sources of signal noise. For these measurements, an on/off cycle was used switching between 0 and 1,000 V every 12 h according to IEC 62788-1-2.[4] The 8008 fixture was placed in an ESPEC BTX-475 environmental chamber enabling measurement as a function of temperature and relative humidity. For polymer measurements, thin films, ~0.46 mm thick, were given at least 24 h to equilibrate to the chamber atmosphere prior to measurement.

Resistivity measurements were performed on commercially available poly (ethylene-co-vinyl acetate, EVA), a thermosetting polyolefin elastomers (POE), and a low iron soda-lime glass with texturing on one side (see Table 1). The EVA and POE were cured using a vacuum lamination cycle, lasting 15 min, with a bed temperature of 145°C. We have not given, and did not obtain, specific information detailing the composition of these encapsulants; therefore, specifically divulging the identity of the materials would not add to the scientific understanding of these materials. The data here are intended to demonstrate typical properties of these classes of materials relevant to leakage current. We had wanted to study polymer effects more thoroughly, but just understanding EVA and POE proved to be more difficult than anticipated. Regardless, EVA and POE are much more relevant to typical PV constructions.

For the glass sample, measuring the surface conductivity requires the flat side to span the annular electrode gap over which the measurement is made (Figure 1). For the glass volume resistivity, however, the textured side could not be used to contact an electrode; therefore, two pieces were laminated together with the smooth side facing outward using an electrically conductive adhesive. The samples were only 50.8 mm × 50.8 mm to fit entirely between the electrodes and cover most of the smaller inner electrode area. This creates a small amount of systematic measurement error because of a small amount of uncontacted area on one side and lateral conduction in the conductive adhesive, but this approximately 5% inaccuracy is unimportant.

Measurements of surface and volume resistivity of these materials were conducted at 25°C, 45°C, and 85°C and at relative humidities of 5%, 50%, and 95% at all of these temperatures. For the glass volume resistivity, the RH was kept low at 5% to minimize measurement error attributable to lateral current flow.

2.2 | One-dimensional transient current measurements in PV cells

The same Keithley 8008 resistivity test fixture and Keithley 6517A electrometer were used for transient current measurements but with a computer recording the data using a LabVIEW program utilizing an IEEE-488 interface. The test coupon was designed to duplicate the current flow characteristics perpendicular to the cell through the glass while ignoring the effects of lateral current conduction across the glass (Figure 2). Cells were cut to 50.8 mm × 50.8 mm squares using a U.S. Laser Corp. Model # 4024/5024 Nd:YVO4 laser scriber operated at double-frequency of 532 nm with a pulse-width of ~5 ns. The glass is cut to 63.5 mm × 63.5 mm squares. The backsheet is a common polyethylene terephthalate containing material. Essentially, no current will pass through the backsheet; therefore, its exact composition is unimportant. The cell is sized such that the corners of the cell extend to the outer diameter of Electrode 2 (Figure 1). The back contact (BC) cells were provided by SunPower, and the front contact (FC) cells were typical industry multicrystalline aluminum back surface mono

	ln (Ro) ln (Ω·cm) or ln(Ω/□)	Ea (kJ/mol)	a (1/% RH)
EVA Resistivity	−5.03 ± 4.89	−102 ± 6	−0.013 ± 0.005
Glass Volume Resistivity	−2.34 ± 0.42	−84 ± 1	NA
Glass Surface Resistivity	−2.70 ± 5.40	−99 ± 14	−0.098 ± 0.012
POE Resistivity	6.56 ± 2.28	−84 ± 6	−0.014 ± 0.005

TABLE 1 Resistivity parameters for all materials tested

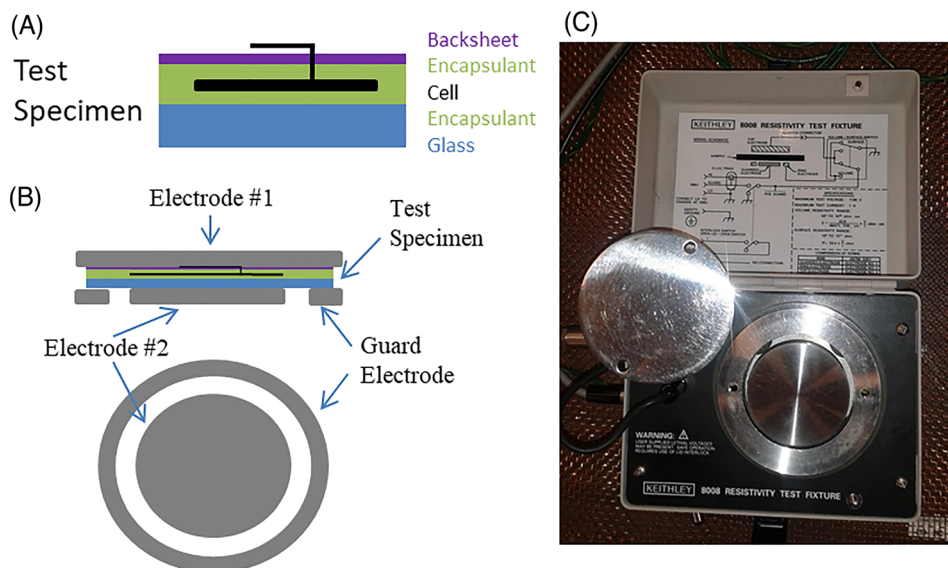*Note*: Determined as a JMP nonlinear fit to Equation (1).

FIGURE 1 (A) Schematic of test specimen. (B) Schematic of electrode. (C) Photograph of electrode fixture
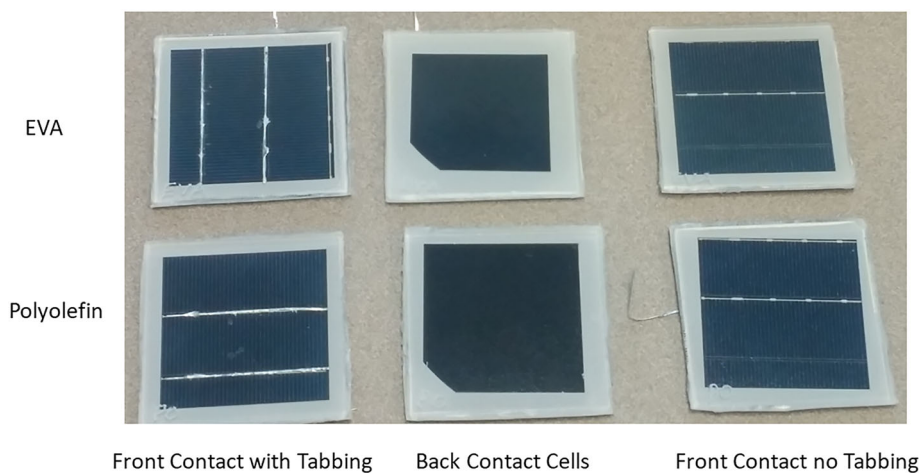

FIGURE 2 Photograph of test samples used in this study. Cells were cut to 50.8 mm × 50.8 mm squares. This contains photos of all the samples used in the study, but several measurements were made on some of the samples under different conditions and at different times.

facial cells. Voltage is applied via some tabbing extending through the backsheet with direct contact with Electrode 1 (Figure 1). While some current can pass from Electrodes 1 to 2 directly past the cell in the perimeter area, this area is much smaller, and the current density is much less than that passing through the cell making it insignificant. With this setup, the effective area is essentially equal to the area of the cell. This provides effectively 1-D current flow between the cell through the encapsulant and glass to the electrode.

2.3 | Two-dimensional transient current measurement in PV cells

In another experiment, a set of single cell mini-modules was created with the same materials but with a conductor placed on the perimeter to simulate a frame (Figure 3B). The frame was grounded, and ±1,000 V was applied to the cell, and the transient leakage current was measured (Figure 3A).

FIGURE 3 (A) Image of a cell with a copper foil used on the edge of the single cell mini-module to simulate a frame. Here, the copper foil is at ground, and the voltage is applied to the cells using the tabs coming out from the backsheet. (B) Schematic of the current flow in a PV module
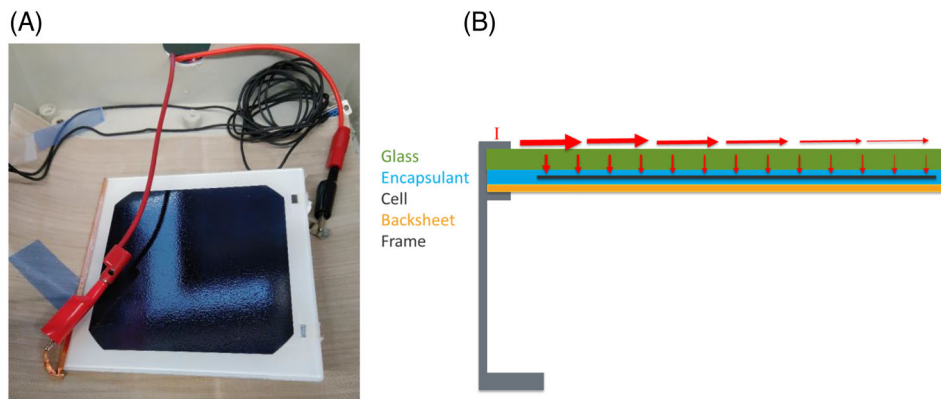
3 | RESULTS AND DISCUSSION

3.1 | Model fit of conductivity/resistivity measurements

The volume resistivity, R, was measured on glass and on two encapsulant materials and were fit to an Arrhenius model[13] as

$$R = R_0 e^{-\frac{E_a}{KT}} e^{RH \cdot a},$$ (1)

where R_0 is a prefactor constant, Ea is the activation energy, K is Boltzmann's constant, RH is relative humidity, and a is a constant related to relative humidity. The surface resistivity for glass was also fit to Equation (1) with $a = 0$. These fits were accomplished using the statistical software JMP such that the uncertainty in the various parameters could also be calculated (Table 1). For these fits, the correlation between $ln(Ro)$ and Ea was always near unity, but the correlation between a and $ln(Ro)$ or Ea was negligibly small. The individual data points for select materials are shown in Figure 2 along with some of the fit lines from Equation (1) and Table 1. This indicates the reasonableness of the model when one considers that getting reproducible measurements within a factor of two for the resistance of insulating materials is good.[20] The only exception to this is for the surface resistivity of glass for which there is a large uncertainty relative to the value. We believe that this is possibly explained by the sensitivity of this surface to contamination.[18] It is also possibly because this is a very different measurement than bulk resistivity and that good contact of the electrodes to the slightly bumpy surface (on the flat side) of the rolled glass may be inadequate.

This large, exponential dependence of resistivity on RH is expected in polymeric materials[7] and can be explained by either the water bonding to ionic species to help separate them from ionic moieties on the polymer, by electrochemical splitting of water to create ionic species for charge transfer, or by plasticization of the polymer backbone.[21] Similarly, the values for the thermal dependence of resistivity are a little higher in EVA compared that of the polyethylene-based material but low relative other more polar polymers generally as reported in the literature[13] (Figure 4).
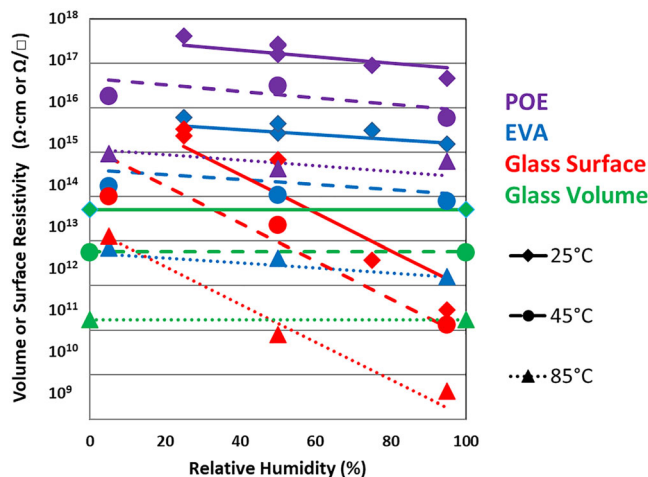

FIGURE 4 Plot of measured and modeled resistivity data for materials examined in this study

A polymer may, depending on the climate, experience humidity from around 10% RH during the day to upwards of 90% RH at night. Seasonal effects further result in about a 30% change in absolute humidity.[22] But because of the high activation energy for resistivity (Table 1), it is the thermal effects that dominate the conductivity of the polymers especially through the diurnal cycles. Therefore, in modeling the leakage current, the contributions from the bulk conductivity of polymeric components are primarily governed by thermal effects. For the glass surface conductivity, however, it is the surface RH that dominates.[8,18]

For a morning temperature increase from 20°C and 100% RH and ending at 40°C and 31.2% RH (assuming the absolute humidity is constant), Table 1 would predict a decrease in the surface conductivity of 63×. This explains most of the reasons that humid environments experiencing a lot of dew are more prone to potential induced degradation and that most of the leakage current is seen in the morning.[8,18,23,24] Higher leakage current is not attributable to moisture absorbed in the polymeric materials. Dew on a module in the morning takes some time to evaporate off, allowing the module to heat up

while maintaining a very high surface RH causing a large increase in conductivity. If only half of the surface is covered with dew, one would see something on the order of a doubling of the conductivity as the water covered areas could be considered highly conductive relative to the dry areas. So even the separation of water droplets would not be expected to dramatically decrease the surface conductivity until the surface is nearly free of condensed water.

This demonstrates how the surface conductivity[25] represents a large source of variability in the leakage current that is highly susceptible to the effects of water and similarly to dust and other pollutants in the air.

3.2 | The nature of current flow, electrons or ions?

At night, the voltage between PV cells and a grounded frame essentially goes to zero, but there is an amount of leakage current resulting from the dissipation of charge in the module. This charge may be a residual effect of capacitance and/or electrochemical reactions. In the experimental setup for samples in Figure 1, the PV cell and Electrode 2 act as the top and bottom of a set of capacitors with some current leakage in the form of the movement of electrons and or ions from material to material. At interfaces, there will be changes in the mobility and concentration of electrons and ions leading to charge build-up. There are also electrochemical reactions at the interfaces anytime the conduction switches between electronic and ionic. This can be the conversion of a water molecule and an electron to hydrogen gas and a hydroxyl group, or hydroxyl groups to oxygen gas, water, and electrons (Table 2). Alternatively, just the nature of the mobile ionic species may change reducing the flow of charge creating charge build-up and consequent electric fields.

An example of interfacial charge build-up was demonstrated at the cell anti-reflective (AR) coating to polymer interface.[9,10,26] While some Na^+ ions have been shown to be able to cross through the AR coating to create shunts in the PV junction,[5] this process is partially reversible through out-diffusion.[27] The reversibility indicates that it occurs without large scale damage, and it is further known that the composition of the AR coating, and its consequent ionic conductivity, is highly influential on a cells resistance to potential induced degradation and preventing the migration of Na^+ ions to the cell.[28] For a good

TABLE 2 Candidate electrochemical and ion exchange reactions possible at various interfaces

Cell at negative bias	Cell at positive bias
Aluminum to glass	**Aluminum to glass**
$3\ OH^- + Al \rightarrow Al(OH)_3 + 3\ e^-$	$\equiv Si\text{-}OH + AlO(OH) + e^- \rightarrow Al(OH)_3 + \equiv Si\text{-}O^-$
$2\equiv Si\text{-}O^- + H_2O \rightarrow 2\equiv Si\text{-}OH + \frac{1}{2}\ O_2 + 2\ e^-$	$Na^+ + Al(OH)_3 + e^- \rightarrow NaOH + AlO(OH) + \frac{1}{2}\ H_2$
$\equiv Si\text{-}O^- + Al(OH)_3 \rightarrow \equiv Si\text{-}OH + AlO(OH) + OH^-$	$Ca^{2+} + 2\ Al(OH)_3 + e^- \rightarrow Ca(OH)_2 + 2\ AlO(OH) + H_2$
	$7\ H_3O^+ + Al_3O_2 + e^- \rightarrow 3\ Al(OH)_3 + 7\ H_2$
Glass to polymer	**Glass to polymer**
$\equiv Si\text{-}O\text{-}Na \rightarrow \equiv Si\text{-}O^- + Na^+$	$\equiv Si\text{-}O^- + Na^+ \rightarrow \equiv Si\text{-}O\text{-}Na$
$\equiv Si\text{-}OH + OH^- \rightarrow H_2O + \equiv Si\text{-}O^-$	$H_3O^+ + \equiv Si\text{-}O^- \rightarrow \equiv Si\text{-}OH + H_2O$
$\equiv Si\text{-}O\text{-}Na \rightarrow \equiv Si\text{-}O^- + Na^+$	$\equiv Si\text{-}O^- + H_2O \rightarrow \equiv Si\text{-}OH + OH^-$
$\equiv Si\text{-}O\text{-}CaOH \rightarrow \equiv Si\text{-}O^- + CaOH^+$	$\equiv Si\text{-}O^- + Na^+ \rightarrow \equiv Si\text{-}O\text{-}Na$
$2\equiv Si\text{-}O^- \rightarrow \equiv Si\text{-}O\text{-}Si\equiv + \frac{1}{2}\ O_2 + 2\ e^-$	$\equiv Si\text{-}O^- + CaOH^+ \rightarrow \equiv Si\text{-}O\text{-}CaOH$
	$\equiv Si\text{-}O\text{-}Si\equiv + H_2O + e^- \rightarrow 2\equiv Si\text{-}O^- + H_2$
	$H_2O + \equiv Si\text{-}O^- \rightarrow \equiv Si\text{-}OH + OH^-$
Polymer to SiN$_x$O$_Y$	**Polymer to SiN$_x$O$_Y$**
$SiN_xO_Y + 2\ OH^- + (1\text{-}y)\ H_2O \rightarrow (SiO_3)^{2-} + x\ NH_3 + H_2$	$SiN_xO_Y + 2\ OH^- \rightarrow (SiO_3)^{2-} + x\ NH_3 + (1\text{-}y)\ H_2O$
$H_2O + e^- \rightarrow OH^- + \frac{1}{2}\ H_2$	$3\ H_2O \rightarrow 2\ H_3O^+ + \frac{1}{2}\ O_2 + 2\ e^-$
$SiN_xO_Y + 2\ Na^+ + (3\text{-}y)\ H_2O + \rightarrow Na_2SiO_3 + x\ NH_3 + 2\ H_3O^+$	
$SiN_xO_Y + H_2O + e^- \rightarrow (SiO_3)^{2-} + x\ NH_3 + (2/3\text{-}x)H_2 + (y\text{-}1)\ H_2O$	
Polymer to gridlines/metallization	**Polymer to gridlines/metallization**
$2\ H_2O + 2\ e^- \rightarrow OH^- + \frac{1}{2}\ H_2$	$3\ H_2O \rightarrow 2\ H_3O^+ + O_2 + 2\ e^-$
$M^{n+} + e^- \rightarrow M^{(n\text{-}1)+}$ (M = Ag, Sn, Pb, Cu ...)	$M \rightarrow M^{n+} + n\ e^-$ (M = Ag, Sn, Pb, Cu ...)
PV cell to AR coating	**PV cell to AR coating**
$Na_2SiO_3 + e^- \rightarrow Na + NaSiO_3^-$	$Si + OH^- \rightarrow \equiv SiH + \frac{1}{2}\ O_2 + e\text{-}$

Note: Red font is for electrochemical reactions, and black font is for ion exchange reactions. Yellow-highlighted items are believed to be the more prevalent reactions. These reactions should be viewed as representative, as there are many different reactions possible and mixed ionic salts or hydrated salts are possible.

AR coating, charged species will accumulate at the polymer to AR coating interface, generating an electric field through the AR coating. There is also a component of the electric field at this surface in the direction of the gridlines.

The resistance of electrons and other charge carriers to crossing the AR coating was notably observed by SunPower, where it was implicated in a reduction in carrier lifetime reductions as a result of surface polarization.[1,26] When the cells were under positive bias, there is a build-up of negative charge on the outside of the AR coating, at the polymer to SiN_xO_y interface. This causes positively charged light-generated holes to accumulate at the front of the cell/AR coating interface where they combine with electrons in the n-type silicon increasing the surface recombination velocity. When stressed in a chamber under bias in the dark, there is an efficiency loss, which is regained upon exposure to light. This indicates that the AR coating becomes photoconductive. Thus, there is evidence of electron movement through the AR coating but with some migration of Na^+ ions through at least some AR coatings. These observations support the idea that there may not be significant electrochemical reactions at the cell to AR coating interface but some minimal electron conductivity in the AR coating allowing electrochemical reactions to occur primarily at the polymer to AR coating interface (Table 2).

At the gridlines, there is both the availability of water molecules and oxidizable metals or conversely, reducible metal oxides. Previously, we showed that under negative cell bias, this results in the corrosion of the AR coating to silicates near the gridlines interface.[9,10] This is presumably either through direct electrochemical corrosion or through the formation of basic species, which enable the corrosion of the AR coating under negative bias. At positive bias, the environment would tend to be acidic, which does not dissolve silicates like a strong basic environment. With positive bias, one would expect to see some dissolution of the gridlines themselves, which has been observed historically when relatively highly conductive polyvinyl butral (PVB) have been used, and to a lesser extent with EVA encapsulants.[9,11,12,29,30]

In the polymer, most of the current conduction is through ionic species, but there would be expected to be some amount of electron based current flow. The difference in the relative contributions could be as high as many orders of magnitude. These ions will be generated or consumed at the glass or at the metallization primarily. But with a material such as glass, if ions are continually removed, a more pure SiO_2 layer will be formed at the interface. This can in turn produce a region resistant to ion flow and hold charged species on both sides, leading to an increase in charging and a reduction in overall conductivity. Being a thin and potentially highly insulating layer, the capacitance can be relatively large. These kinds of effects can also change the nature of the conduction to favor the movement of electrons over ions.

Na^+ is not the only species that can flow through the polymer, but it is the primary one implicated in PID degradation of Si cells because of its mobility, approximately 15 weight percent Na_2O in glass, and through its specific ability to incorporate itself into the crystalline lattice.[5,6,15–17] Other possible conductive species include OH^-, H_3O^+, K^+, Ca^{2+}, $Fe^{2+,3+}$, Ag^+, and Mg^{2+}. Presumably, these other species are not easily incorporated into the Si lattice, and/or their effects are less important.

The relative contributions of these different species is unknown, but smaller and monovalent ions would be more mobile, and of course, higher prevalence would be a significant consideration too. The direction of flow is dependent on the bias and on the charge of the species. For OH^- and H_3O^+, this is important because they can be produced at different interfaces and move in the opposite directions to produce the same net current. Species like Fe and Ag can be plated out on surfaces, but Ca and Mg are reactive such that they would be expected to oxidize upon reaction with water to form hydrogen gas and hydroxides, which could further diffuse down concentration gradients.

In soda-lime glasses, the dominant form of conduction is through smaller monovalent cations, most notably Na^+. Because of this, it is expected that the electrochemical reaction enabling the change from electron to ion conduction occurs almost exclusively at the Al-frame to glass interface. Depending on the bias, this is primarily the result of either Na^+ motion and/or $\equiv Si-O^-$ production in the glass to redoxively produce H_2 or O_2 at the Al frame interface or to oxidize Al when the cell is at negative bias. At the glass to polymer interface, primarily, ion exchange reactions are occurring. This can result in the removal/addition of Na^+ or other cations from/to the glass or the production/consumption of OH^- in the polymer. If Na^+ is removed from the glass, it will be depleted from the surface, resulting in the formation of a more highly resistive layer,[2] which may in turn result in charge build-up at its interfaces.

3.3 | Electric field driving forces for transient voltage relaxation modeling

In the test samples (Figures 1 and 2), current conduction is essentially one dimensional. In a PV module, the current must travel laterally across the glass before going through the glass and polymer to the cell. The resistivity in the polymer is so much greater than the glass (Figure 4) that there is no significant lateral conduction in the polymer. Comparison of the glass surface to the bulk conduction is complicated; however, the observation that the morning dew has a large effect on the total current flow[8,10,18,23,24] and the observation that potential induced degradation is seen mostly but not exclusively on the perimeter cells[31–34] confirm that glass surface conduction is the dominant lateral conduction pathway.

As discussed earlier and in other publications,[10,19] the current flow at the AR coating is complicated because it is much more resistive than the polymer, which allows for charge build-up, but also for the leakage current to flow to the gridlines where electrochemical reactions occur causing conversion of SiN_xO_y into Na_2SiO_3. For simplicity, however, we are modeling our test cells (Figure 2) mostly as 1-D capacitors.

For a capacitor, the capacitance (C) is given by

$$C = \varepsilon_r \varepsilon_o \frac{A}{d} \tag{2}$$

where A is the area, d is the distance through the electrical insulator, ε_o is the permittivity of free space, and ε_r is the relative permittivity of

the insulator (Table 3). The cell can be thought of as a series of capacitors each in parallel to resistors, which allows leakage across the capacitors. However, this cannot be modeled as a simple series of capacitor/resistor pairs because the "capacitors" are composed of shared charge located at an interface. Thus, it is more appropriate to model the charge accumulation at the outer glass (Q_G), glass/polymer (Q_P), polymer/AR coating (Q_{AR}), and the cell to AR coating (Q_C) represented as areal charge densities.

For a deployed module at a positive charge, there can be a net charge on it with current flow from the center of the module to the grounded frame. It is not until one draws an imaginary boundary around enough of the system that the net charge will be zero. For our test sample coupons, we assume that the interfaces are infinite planes with one side electrically grounded. Here, charge will accumulate at the various interfaces such that the sum total of the charge is equal to zero,

$$Q_G + Q_P + Q_{AR} + Q_C = 0. \tag{3}$$

At steady state, this charge will be in the form of electrons or holes in the cell and primarily ionic species in the other layers of the same net but opposite charge.

Making an assumption that the charge is effectively in the form of an infinite plane, then the electric field, which is the force (F) exerted on a particle with a charge (q), in each layer is given by

$$\vec{E} = \frac{F}{q} = \frac{V}{t} = \frac{Q_2 - Q_1}{2 \cdot \varepsilon_r \varepsilon_o}, \tag{4}$$

where V is the voltage difference between the two interfaces, t is the distance between the two plates, and the Qs are the charge densities on the opposite sides of the two interfaces but not necessarily at the interfaces. For sets of infinite planes of charge with a net zero charge, the electric field outside of the furthest plane is zero. For a typical capacitor, the positive and negative charges on the two capacitors are equal and opposite, allowing the factor of ½ and one of the Qs to be eliminated in a similar equation. Electric fields obey the law of superposition, meaning that the composite electric field from two or more sets of charge pairs can simply be summed up. Because the

negative charge on the cells must be balanced by an equal positive charge at the relevant interfaces, the contribution to the total electric field is just the ratio of that charge to the permittivity. With this, the electric field in the glass (E_G), polymer (E_P), and AR (E_{AR}) layers are given by

$$\vec{E}_G = \frac{Q_G}{\varepsilon_G \varepsilon_o}, \ \vec{E}_p = \frac{Q_G + Q_P}{\varepsilon_P \varepsilon_o}, \text{ and } \vec{E}_{AR} = \frac{Q_G + Q_P + Q_{AR}}{\varepsilon_{AR} \varepsilon_o}, \tag{5}$$

where the subscripts G, P, and AR refer to the properties of the glass, polymer, or AR coating, respectively. The product of the various electric fields and the distance results in a voltage drop. This static charge serves to counteract the flow of charge through the cell layers. The sum total of the static voltage is given by

$$\begin{aligned} V &= \frac{t_G Q_G}{\varepsilon_G \varepsilon_o} + \frac{t_P(Q_G + Q_P)}{\varepsilon_P \varepsilon_o} + \frac{t_{AR}(Q_G + Q_P + Q_{AR})}{\varepsilon_{AR} \varepsilon_o} \\ &= \frac{Q_G}{C_G} + \frac{(Q_G + Q_P)}{C_P} + \frac{(Q_G + Q_P + Q_{AR})}{C_{AR}}. \end{aligned} \tag{6}$$

This total voltage can be expressed in terms of the ratio of the net charge on both sides (not just charge immediately on the surface) to the capacitance of the various layers. The resistivity of the glass is several orders of magnitude lower than the polymer, which results in $Q_G \ll Q_P$ because only a very small voltage drop across the glass will reduce the charge differential and the charge will have a much more difficult time traversing the polymer. Therefore, the first term in Equation (6) is essentially negligible at steady state, and there is an insignificant amount of charge at the outer glass interface, Q_G. At steady state, the only significant voltage across the glass is associated with the flow of current.

3.4 | Glass resistivity estimation

Prior to turning on the voltage, it can be assumed that essentially all of the charge has been dissipated. When the voltage is turned on, there will be some charge build-up on the two electrodes associated with the Keithley measuring instrument and the whole sample, but this is so fast that its effect is not measureable and may be neglected. The resistance

TABLE 3 Test sample modeling dimensions and characteristics

Component	Relative permittivity	Thickness	Layer capacitance (nF)	Resistance at 23°C and 50% RH (Ω)
Glass	7.75	3.2 mm	0.055	$7.7 \cdot 10^{11}$
Glass AR Coating	5	200 nm	570	Unknown
Silica	3.8			
Si_3N_4	7.5			
EVA	2.3	0.46 mm	0.11	$1.7 \cdot 10^{14}$
POE				$1.1 \cdot 10^{16}$

Note: Permittivity values were obtained as estimates from typical literature values. Capacitance calculated according to Equation (2). Resistance calculated using parameters from Table 1.

across the glass is much less than across the polymer; therefore, the initial transient response can be expected to function as a simple series RC circuit. Here, the initial current is determined by the ratio V/R because an uncharged capacitor acts as an open circuit. As the capacitor charges up, a voltage builds up to oppose the flow of current, leading to an exponential decay in current for a simple RC circuit as

$$I(t) = \frac{V}{R}\left(1 - e^{-\frac{t}{RC}}\right). \tag{7}$$

In our test cells, this holds approximately true for short time frames where the equivalent resistor is that of the glass and the short time capacitance (C_o) is given by

$$C_0 = A\varepsilon_o \left(\frac{\frac{\varepsilon_P}{t_P}\frac{\varepsilon_{AR}}{t_{AR}}}{\frac{\varepsilon_P}{t_P} + \frac{\varepsilon_{AR}}{t_{AR}}}\right) \approx A\varepsilon_o \left(\frac{\frac{\varepsilon_P}{t_P}\frac{\varepsilon_{AR}}{t_{AR}}}{\frac{\varepsilon_{AR}}{t_{AR}}}\right) = \frac{A\varepsilon_o\varepsilon_P}{t_P} = C_P. \tag{8}$$

The thickness of the AR layer is so relatively thin that when looking at the overall capacitance, it can be ignored. For this series RC circuit, the logarithm of the initial decay in current flow can be used to estimate the resistance of the glass (R_G) as

$$R_G = \frac{t}{[ln(I_o) - ln(I)]C_o} \approx \frac{t_2 - t_1}{[ln(I_1) - ln(I_2)]C_P}. \tag{9}$$

Because it is not possible, with the equipment we used, to measure the current at the instant the measurement begins, we use the first two data points, which are at best at 2.6 and 3.4 s, or for the worst case scenario, of a FC +1,000 V without solder run (Table 4), where the first two points were at 46.6 and 47.5 s. The use of secondary points is theoretically valid for a system with just one capacitor and one resistor so long as the charge has not yet built up on the AR-polymer interface. The characteristic time constant for charge build-up on the AR coating is given by $R_P \cdot C_{AR}$, which is approximately $2.52 \cdot 10^{10}\ \Omega \times 5.71 \cdot 10^{-7}\ F = 14,000$ s, substantiating the idea that this is not significant at these short time scales.

Charge accumulation in the interior layers of the samples is not expected to affect these initial measurements according to Equation (9). This assumption is validated by the consistency of these time constant measurements in Table 4 for all cell and encapsulant configurations when comparing the voltage-on transitions or voltage-off transitions to each other but not when comparing voltage-on to voltage-off transitions. The independence from the cell geometry and encapsulant type indicates we are indeed measuring the effects of the initial charging at the glass to polymer interface. The voltage-off transient current time scale is about 1.4 s as opposed to 4.0 s, which cannot be explained by a change in the capacitance of the encapsulant but must therefore indicate the glass resistance after charging. This increase in the glass resistance by 2.9× upon voltage exposure may help to explain some of the observed higher current in modules in the morning.[35] This increase is most likely the result of the depletion of charge carriers in one of the glass surfaces creating a more resistive and purer SiO_2 surface layer.

The glass resistance can also be estimated from the initial current as the ratio of V/I_o, Equation (7). However, the electrometer can only measure the resistance after a finite time of a few seconds making the resistance estimate systematically high with this method. On average, this produced resistances that were 59% higher than when using the initial slope in Equation (9). This is consistent with time scales being on the order of 4 to 1.4 s and the measurements being made a few seconds after the switching of the voltage. We did not see statistically significant differences between the different configurations. Similarly, we did not see a statistically significantly different difference between R_G measured from the initial voltage-on or from the voltage-off current measurements. This contrasts with the estimate made using Equation (9), which did show differences, but the standard deviation was 36% and 20% for on versus off measurements (Equation (9)) as opposed to 98% and 57% for on versus off measurements (first measured current). We believe the inability to find a difference here is related to the experimental variability, which could be fixed or mitigated by better sampling and statistics, but the decay time method is clearly the preferred method to do this.

The simplistic 1-D models underlying Equations (4)–(6) and (8) have some concerns with some relevant 3-D aspects. In particular, the metallization requires another assumption to be applied to this model framework, which has some validity concerns because the spacing is of a relevant width compared to the encapsulant thickness. In the FC cells, the metallization also traverses the AR coating and penetrates into the polymer layer. The relevant thickness for the glass, encapsulant, and AR coating are approximately $d_G = 3.2$ mm, $d_E = 0.46$ mm, and $d_{AR} = \sim 200$ Å, respectively (Table 3). In these cells, the metallization spacing was ~ 1.16 mm, the width is about ~ 0.050 mm, and the height is around ~ 0.040 mm.

Earlier,[9,19] we demonstrated that the electrochemical reactions on the cell surface result in the formation of sodium silicates near the gridlines. This indicates that the current flows to the AR coating and builds up a charge, with the AR coating acting as a capacitor/insulator. Then, some of the current flows laterally to the gridlines. The BC cells have no front side gridlines and have been shown to have pronounced charging effects. In our experiments, it was found that the BC cells had generally lower steady-state voltage-on leakage currents (Table 4), indicating the dominance of the pathway of charge flowing through the metallization as opposed to flowing through the AR coating. In Swanson et al.,[26] they explain that the presence of light serves to make the AR coating photoconductive, which allows the charge to dissipate. This is an electronic mode of charge transfer, indicating that there must necessarily be electrochemical reactions occurring at the AR coating to polymer interface. Noting that the conversion of silicon oxy-nitride to silicates is not reported, the more dominant electrochemical reaction is the splitting of water into either hydroxide or hydronium ions, which does not appear to rapidly corrode the surface. It is likely that the basicity in the polymer is simply not strong enough and/or hydroxide ions are being converted elsewhere to oxygen and water to partially neutralize the chemistry. In the BC cells, the lower currents (Table 4) also indicate that these electrochemical reactions are less pronounced relative to the FC cells. We assume these

TABLE 4 Transient current characteristics of test samples

Cell type	Solder and tabbing	Encapsulant	Voltage (V)	Voltage-on steady state current (nA)	Voltage-on cycle charge (mC)	Voltage-off cycle charge (mC)	Voltage-on initial current measurement at ~2.4 s (nA)
BC	NA	EVA	+1,000	0.91	0.039	0.00085	6.1
BC	NA	EVA	+1,000	0.95	0.041	0.0012	6.2
BC	NA	EVA	+1,000	3.7	0.16	0.0043	21
FC	No	EVA	−1,000	4.7	0.21	0.0023	32
FC	No	EVA	+1,000	4.7	0.20	0.0013	23
FC	Yes	EVA	+1,000	11	0.75	0.00024	52
FC	Yes	EVA	−1,000	7.3	0.39	0.0024	39
FC	Yes	EVA	+1,000	20	0.89	0.031	47
FC	Yes	EVA	1,000	15	0.66	0.0021	35
BC	NA	POE	+1,000	1.5	0.090	0.00041	22
FC	NA	POE	+1,000	NA	NA	0.00026	53

Note: Data from the first voltage-on cycle were ignored in these calculations. For most samples, only one measurement was made, but for some, duplicate measurements were made and sometimes with different cycle times as indicated.

TABLE 4 (Continued)

Cell type	Voltage-off initial current measurement at ~2.4 s (nA)	Voltage-on apparent glass resistance from initial current measurement, equation 5 (Ω)	Voltage-off apparent glass resistance from initial current measurement, equation 5 (Ω)	Voltage-on time constant 1/RC, equation 7 (1/s)	Voltage-off time constant 1/RC, equation 7 (1/s)	Voltage-on glass volume resistivity from short time RC slope, equation 9 (Ω)	Voltage-off glass volume resistivity from short time RC slope, equation 9 (Ω)	Comment
BC	8.7	$1.6 \cdot 10^{11}$	$1.1 \cdot 10^{11}$	5.74	1.52	$5.0 \cdot 10^{10}$	$1.3 \cdot 10^{10}$	Two, 4 h cycle
BC	8.8	$1.6 \cdot 10^{11}$	$1.1 \cdot 10^{11}$	5.94	1.52	$5.2 \cdot 10^{10}$	$1.3 \cdot 10^{10}$	Two, 5 h cycles
BC	21	$4.8 \cdot 10^{10}$	$4.8 \cdot 10^{10}$	2.77	1.41	$2.4 \cdot 10^{10}$	$1.2 \cdot 10^{10}$	
FC	30	$3.1 \cdot 10^{10}$	$3.3 \cdot 10^{10}$	2.73	1.64	$2.4 \cdot 10^{10}$	$1.4 \cdot 10^{10}$	
FC	26	$4.4 \cdot 10^{10}$	$3.8 \cdot 10^{10}$	3.46	1.51	$3.0 \cdot 10^{10}$	$1.3 \cdot 10^{10}$	
FC	9.4	$1.9 \cdot 10^{10}$	$1.1 \cdot 10^{11}$	6.33	1.72	$5.5 \cdot 10^{10}$	$1.5 \cdot 10^{10}$	Three cycles
FC	34	$2.6 \cdot 10^{10}$	$2.9 \cdot 10^{10}$	2.89	1.73	$2.5 \cdot 10^{10}$	$1.5 \cdot 10^{10}$	
FC	29	$2.1 \cdot 10^{10}$	$3.5 \cdot 10^{10}$	3.24	0.83	$2.8 \cdot 10^{10}$	$7.3 \cdot 10^{9}$	
FC	22	$2.9 \cdot 10^{10}$	$4.5 \cdot 10^{10}$	4.73	1.13	$4.1 \cdot 10^{10}$	$9.9 \cdot 10^{9}$	Three cycles
BC	21	$4.6 \cdot 10^{10}$	$4.8 \cdot 10^{10}$	2.54	1.21	$2.2 \cdot 10^{10}$	$1.1 \cdot 10^{10}$	
FC	22	$1.9 \cdot 10^{10}$	$4.5 \cdot 10^{10}$	3.21	NA	$2.8 \cdot 10^{10}$	NA	Inconsistent data

Note: Data from the first voltage-on cycle were ignored in these calculations. For most samples, only one measurement was made, but for some, duplicate measurements were made and sometimes with different cycle times as indicated.

electrochemical reactions are much more easily catalyzed on the metallization as opposed to the AR coating. Thus, standard front metallization cells would be expected to be in a more corrosive environment (i.e., more extreme high or low effective pH).

3.5 | Simplified schematic for current flow modeling

A rough schematic of the current flow is shown in Figure 5. Here, the lateral current flow, illustrated as flowing from the AR coating to the metallization, can be assumed to dominate over the current flow through the AR coating such that in a modeling effort, flow through the AR coating can be essentially ignored. Because of the relatively small height and width of the metallization compared to the thickness of the encapsulant and as we will see, the variability in the resistance values, this penetration of tabbing into the encapsulant was ignored.
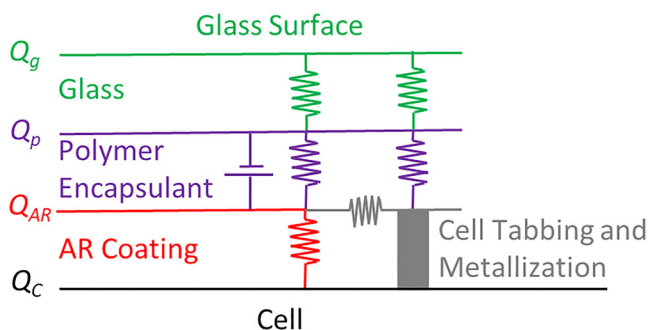

FIGURE 5 Schematic of electrical circuit for conduction of current through the cell. This model is not intended to be an exact representation but just to illustrate the primary charge sources and effective pathways.

The thickness and spacing of the metallization are of the same order of magnitude making the 2-D nature of the electric field still impact current flow to the metallization.

To evaluate the current flow to the metallization in the FC cells, we must consider the voltage above the AR coating and on the glass to polymer surface. In Table 4, we show the steady state current in the voltage-on state, which for 50.8 cm × 50.8 cm cell test samples averages to $1.05 \cdot 10^{-8}$ A and $1.75 \cdot 10^{-9}$ A for FC and BC, respectively. Thus, a rough estimate would be that about 1/6th of the current is flowing through the AR coating in the FC cells. When exposed to light, some increase in the photoconductivity of the AR coating would be expected to reduce this ratio of current pathways. To estimate the maximum voltage drop across the AR coating in the FC cells, one could assume a maximum charge build-up in the center of the cell then lateral current flow across the AR surface with charge density decreasing to a value, which is still non-zero, at the metallization interface. There is a problem with making this estimate of the relative current flow through the AR coating, and through the metallization, we do not have a way to estimate the amount of charge build-up around the gridlines. When the voltage is turned off, $5.68 \cdot 10^{-6}$ C and $1.68 \cdot 10^{-6}$ C are dissipated for the FC and BC cells, respectively. However, the standard deviation for these measurements is between 103% and 198%, making this difference insignificant. This can be interpreted as the presence of the AR coating does not affect the charge build-up, that there are relevant differences in the AR coatings (from different manufacturers), and/or that the transient behavior and chemistry is dramatically different.

The schematic shown in Figure 5 can be simplified for the BC cells as a removal of the metallization, making it a 1-D current flow model. For FC cells, the presence of gridlines does not seem to have an effect on charging that is larger than many of the other variabilities in the current flow and can be thought of as an uncertainty in the charge path length, where it is effectively about 50% longer at most. Therefore, for the purposes of more rigorous modeling to elucidate

FIGURE 6 Steady state voltage-on current for minimodules with a metal foil frame under applied voltage to the cell. The data point for FC cells at +1,000 V in PO was simply not taken.
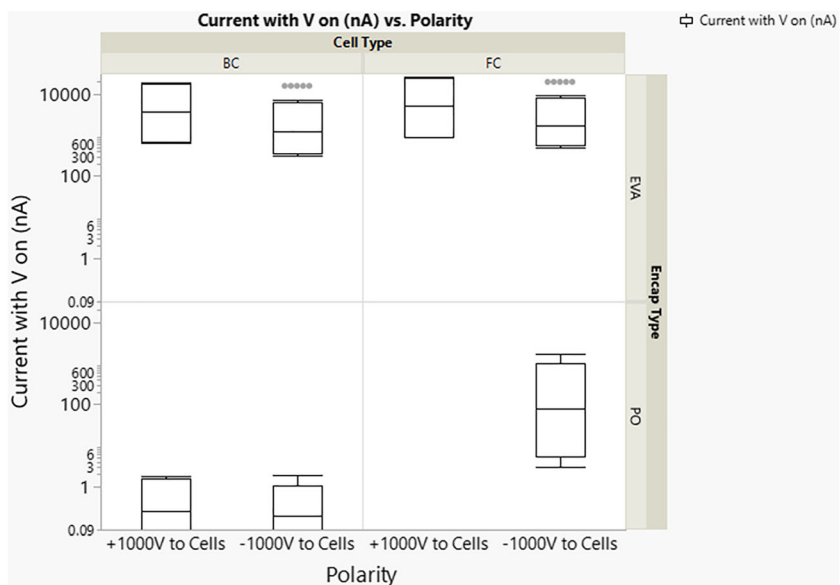
more information about current flow, we will assume the FC cells to be primarily 1-D in nature.

3.6 | Measurements of current flow from a frame

In the experiment using a copper foil to represent a frame (Figure 3), when EVA was used, the difference between the applied voltage and the cell type was irrelevant (Figure 6). But for the PO encapsulant, there was a significant difference between the FC and BC cells. It is known that Na^+ is a significant contributor to PID and that EVA provides better conductivity to Na^+ than does PO, even when the overall conductivity of the two polymers is comparable.[15–17] The difference (Figure 6) is likely due to the presence of metallization, but the observation that both positive and negative biases had similar conductivity for the BC cells indicates that this phenomena is not just attributable to the presence of Na^+. There must be other ions that have conductivities that are sensitive to polymer type and experience electrochemical interactions with the metallization. We hypothesize that the metallization allows for electrochemical reactions to occur more easily and that with the BC cells, there is a build-up of ions resisting the flow of current.

3.7 | Effects of multiple charge carrier types

For the 1-D test samples (Figure 2), we typically ran the charge/discharge cycle five times for a length of time of 12 h for both the voltage-on and voltage-off phase of each cycle to duplicate a typical diurnal cycle. The first charge cycle typically differed from the rest, but good consistency with the remaining cycles was typically obtained (Figure 7). For all samples tested, the terminal discharge values were almost always in the upper 10^{-11} A range, and the steady-state voltage-

on current was between $9 \cdot 10^{-10}$ A and $2.00 \cdot 10^{-8}$ A (Table 4). During charging, there is a fast reduction in current leading to a plateau value. Then, in the voltage-off phase, there is an initial fast decay followed by a slower decay at very low currents. This indicates the presence of at least two important species or processes with different time scales. We also assumed that the instrumental response and the response time for dipole moment reorientation were much faster than the 2.4 s required for the first data point to be recorded and where thus ignored.

As a first attempt at modeling the complete current flow, the sample is modeled with an electric field across the glass, polymer, and AR layers according to Equations (5) and (6). This is essentially using the capacitance of these layers in conjunctions with charge build-up at each of the interfaces. Then, current is allowed to pass through the layers with the glass being modeled as having a constant resistance. However, the shape of the discharge curves, for example, Figure 7, clearly indicates the transport of at least two important species or processes with different time scales as seen by the dramatic change in the slope. This is relevant at time frames greater than 0.1 h (360 s), but the glass charging process has a characteristic time on the order of about 1.4 s and no indication of secondary processes. Thus, the location of this multiplicity of charge carrier processes is predominantly associated with the polymer layer. To model this, we modeled three different species with a different mobility ($1/R_{P1}$, $1/R_{P2}$, and $1/R_{P3}$) such that the electric field across the polymer is calculated according to Equation (5) from which the charge transfer is calculated and separately accumulated at the polymer AR coating interface for the three species separately. Here, it should be noted that the build-up of charged species can be from the production of positive and negative species with one leaving or equally from the influx of either a positive or negative species. For this analysis, it is assumed that there is an infinite supply of charged species. This is true for species coming from the glass or for those derived from the splitting of water. In Equation (5), the total electric field is calculated from the sum of the contributions from the various species. Furthermore, the driving force for the loss of a given species at the polymer-AR coating interface (R_{L1}, R_{L2}, and R_{L3}) is proportional to the amount of charge accumulation of that species and the voltage from there to the cell. Again, the voltage is determined from the sum of the electric charge and applied to each charged species separately with a different loss factor. But when one accounts for both these factors, the leakage current is just proportional to the concentration of the particular charged species. This loss of charge carrier is either by migration to the gridlines or through the AR coating and does not differentiate between electronic flow through the AR coating with electrochemical reactions at the interface or lateral movement to the gridlines where an electrochemical reaction can happen according to one of the scenarios in Table 2.

If one fixes the capacitance across the glass as estimated in Table 3 and uses the value for glass resistance (Table 4) as the average from the voltage-on and voltage-off slopes according to Equation (9), the other parameters (Table 5) can be adjusted to yield a reasonable representation of the curves in Figure 7 (red and green markers). The leakage current resistance values in Table 5 have units of [$\Omega \cdot C$] because the leakage rate of a particular charge carrier in this model is
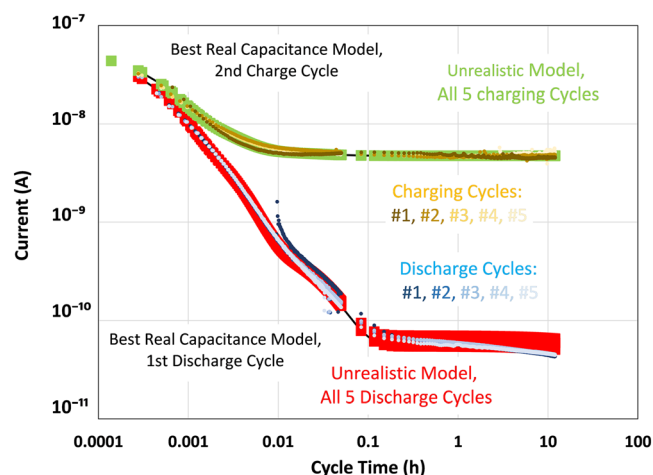

FIGURE 7 Transient current measurements for a FC cell with solder and EVA. The fit used here (red and green markers) required unrealistic capacitance values to work. The parameters for these fits are indicated in Table 5.

related to the amount of it present. With a remaining unrealistic value for the capacitance of the AR coating, one can obtain a reasonable fit to the data. It takes two different species in the charging part of the cycle to get the curve to match and a third one, which is unnoticeable in the charging cycle, to get the long term discharge characteristics.

The movement of minute amounts of charge will not affect the permittivity of the various components or the capacitance of that layer (Equation 2). As demonstrated earlier, the high resistance of the polymer relative to the glass requires the initial part of the charging curve to be dictated by the current flow through the polymer. Until a counter acting voltage is being built up on the AR coating, or the current flow has decreased to near the steady state where significant current is traversing the polymer, the slope on a semi-log curve cannot deviate from a straight line (Figure 8A). Because the AR coating capacitance is about 5,000× larger than the polymer capacitance, and because flow to it through the polymer is orders of magnitude smaller than flow through the glass, a counter acting electric field cannot be produced in the AR coating till much longer time scales. With this model, it is not possible to match up the slope of the charging curve at both the initial times and at intermediate times prior to approaching steady state with a constant resistance in the glass. Therefore, on time scales of around 30 s, the resistance in the glass must be increasing during charging. Because the modeled steady-state current is about 2.4× higher than the measured current in Figure 8A, the glass resistance must be increasing quickly. Then, upon removal of voltage, the resistance reversibly decreases by about 2.4×.

The leakage current clearly shows three distinct time scales for current flow, >0.4, 0.4 to 0.1, and <0.1 h (Figures 7 and 8). At short times, the leakage current is necessarily higher than predicted because it is still governed by the resistance of the glass. Even if during discharge the model uses lower glass resistance, as predicted by the initial slope, there is not enough current to match the measured current. If parameters are changed to produce more charge storage from the more mobile charge in the polymer, then it does not decay to negligible time scales after 0.1 h as measured. Clearly, there are other forces or changes in the relevant parameters. Similar curves and similar difficulties were seen in most of the other samples. The only exceptions to this are discussed in the next section. The simple capacitance and constant resistance models just cannot explain this data set. As the cell discharges, the resistance to current increases, or, alternatively, the driving force decreases dramatically through other driving forces.

3.8 | Effects of chemical concentration gradients

The resistance in the glass goes up as a function of charging, which can easily be explained by the formation of resistive layers depleted from alkali elements. This can happen despite an essentially infinite source of ions in the glass. However, when the voltage is removed, the initial current flow is higher, and the resistance of the glass from RC measurements is lower than in the voltage on transition. This indicates the presence of additional driving forces for current flow, which

TABLE 5 Parameters for current leakage modeling attempts in Figure 7

Configuration description	R_g (Ω)	C_p (nF)	R_{p1} (Ω)	R_{L1} (Ω·C)	C_{AR} (nF)	R_{p2} (Ω)	R_{L2} (Ω·C)	R_{p3} (Ω)	R_{L3} (Ω·C)
FCC, −1,000 V, EVA no tabbing, unrealistic capacitance	$1.80 \cdot 10^{10}$	0.11	$5.50 \cdot 10^{10}$	$5.70 \cdot 10^{10}$	0.40	$9.00 \cdot 10^{11}$	$2.70 \cdot 10^{11}$	$2.00 \cdot 10^{16}$	$1.50 \cdot 10^{15}$
FCC, −1,000 V, EVA no tabbing, realistic capacitance	$1.80 \cdot 10^{10}$	0.11	$7.00 \cdot 10^{10}$	$5.00 \cdot 10^{10}$	57,100	$2.00 \cdot 10^{131}$	$1.50 \cdot 10^{11}$	$15.0 \cdot 10^{16}$	$1.74 \cdot 10^{15}$

Note: Parameters are determined either empirically, from measurements (Table 4) or from typical material parameters (Table 3).
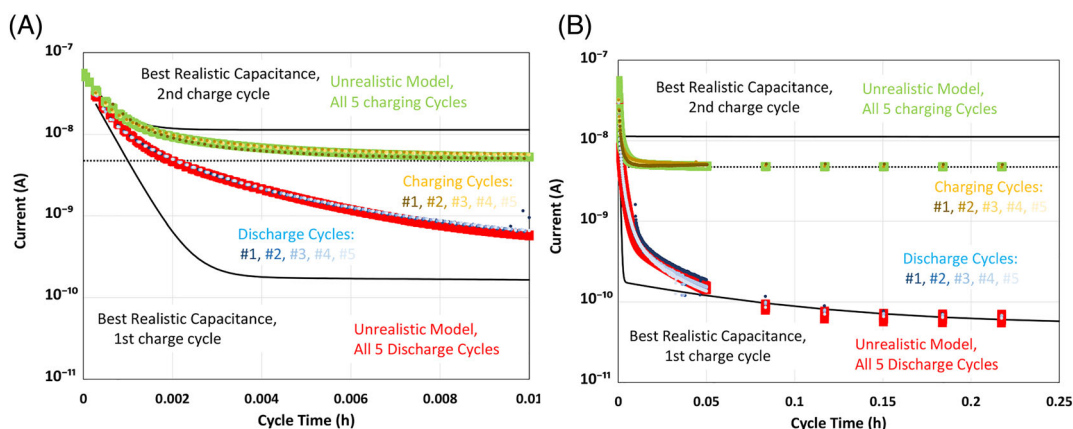

FIGURE 8 Transient current measurements for a FC cell with solder and EVA. The fit used here (red and green markers) required unrealistic capacitance values to work. Shown on a semi-log plot with different time scales to accentuate the appearance of different transient current time scales. (A) Short timescale. (B) Long time scale.

we believe are due to chemical potential effects. The Nerst equation explains how the activity (or chemical potential) of a species is related to the voltage potential in an electrochemical cell. Because the oxidative and reductive activity (a_{Ox} or a_{Red}) is affected by concentration, the depletion of ions in the glass surface layer produces a voltage driving the system toward equilibrium as

$$V = \frac{RT}{F} ln\left(\frac{a_{Ox}}{a_{Red}}\right) = \frac{RT}{F} ln\left(\frac{[Ion\ Concentration\ Electrode\#1]}{[Ion\ Concentration\ Electrode\#2]}\right), \quad (10)$$

where R is the universal gas constant, T is temperature in Kelvin, and F is the Faraday constant. In the context of a PV cell, this could be exemplified as [OH^-], which would drive a water splitting reaction at the two electrodes producing O_2 and H_3O^+ at one electrode and H_2 and OH^- at another to equilibrate the relative hydroxyl concentration, [OH^-]. Similarly, any of the other electrochemical reactions in Table 2 could be important. Because of this, when the voltage is turned off, there is an additional driving force for current flow resulting from the gradient in ion concentration in the glass. When considering the time scale from an RC current, this would manifest as an apparently higher leakage current or lower resistance as was seen.

Conversely in the polymer encapsulant (middle time scales; Figures 7 and 8), the initial current drops off more slowly than one would expect. The magnitude of the effect cannot be explained by just a recovery of the higher conductivity in the glass. The product of the glass resistance and the polymer capacitance gives a time scale of 1.4 and 4.0 s from the initial voltage-off and voltage-on current decay curves, respectively. To see a 95% reduction of the initial current would take between 4 and 12 s (0.0011 and 0.0033 h in Figures 7 and 8). Because the time scale for accumulation of charge at the glass/polymer interface is too fast to explain the current decay characteristics, there must be another source of current that is significant and long lived in the polymer.

An infinite series of different charged species with different decay times and magnitudes discharging through the polymer could be made to fit this decay curve. Such a model is purely empirical and thus not useful for understanding the underlying physics. It also implies that there is not a single or even a few species that could be used to simply explain the curve. Attempts were made with three moving charged species, but this could not be used to predict the curve especially when one must acknowledge that the bulk of the initial current flux was from charge already located at the glass to polymer interface.

The increase in resistivity upon application of a DC voltage is a well-known phenomena in polymers and insulating materials.[36,37] The polymer is highly depleted of charge carriers at the end of the voltage-on cycles, and the glass would have higher concentrations of carriers at one side and lower concentrations at the other with the middle essentially unchanged creating an opposing electric field. Furthermore, Equation (10) describes a restoring voltage due to differences in chemical potential of concentration of ions across the polymer. It is easy to imagine the concentration of these ions differing by orders of magnitude generating substantial voltages especially considering that the charge separation was created using 1,000 V. If there was a 100× difference in ion concentration or equivalently ion

activity, this could produce a 0.12 V driving force across the polymer to the grounded metallization or across the glass. This voltage is much smaller than the initial voltages from charge accumulation at the interfaces, and with a glass resistivity of around 3.0 10^{10} Ω, the chemical potential induced voltage drop across the polymer cannot account for the excess discharge current for up to 0.05 h. But if it was a little higher than 0.12 V, it could explain the terminal discharge current. However, in the glass sufficient charge accumulation at the glass polymer interface could explain some of the initial (<0.05 h) excess current flow. Even if the charge at the glass polymer interface was not there, the chemical potential induced voltage across the polymer may help explain the current flow across the glass. Current from an electrochemical potential would look like an initial shunting leakage pathway for this charge to flow past the glass. This added current would dissipate as the charge at the polymer to glass interface, diminishing the relevant chemical potentials. This could be a partial explanation of the persistent higher measured leakage current, which is not explained by the simplistic model of Figure 5.

3.9 | Unexpected discharge reversal

It was reported earlier that with some samples, the discharge current was initially a negative current after application of positive current and positive bias but that the sign of the discharge current switched to a positive current after some time.[10] This was seen in both the EVA and POE but was more commonly seen with the POE. In that work, the electrometer measuring four different samples simultaneously was switched around, reproducing a continuation of the anomalous current flow on the four different samples of which two were showing the anomaly. This eliminated the possibility that this was an artifact of a
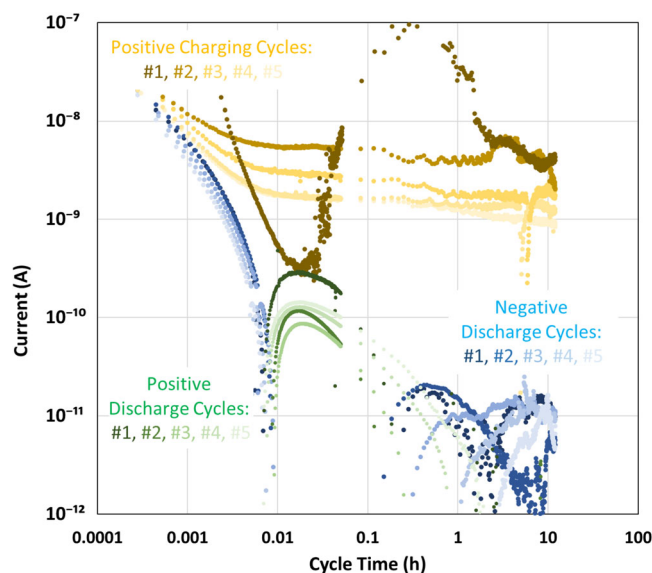

FIGURE 9 Transient charge and discharge current for a BC cells at +1,000 V with a POE encapsulant. This shows repeatable anomalous discharge behavior.

particular instrument. Furthermore, the observed reversal was repeated several times on different samples. All of those measurements were performed at SunPower. At NREL, using different samples, a different electrometer, and a different location, this counterintuitive behavior was also observed, indicating it is not just an experimental anomaly (Figure 9). A reversal of current flow cannot be simply a charging effect and because of the repeatability from cycle to cycle, and the fact that it does vary up and down a bit, indicates it is not just stray charge from another experiment on the same sample.

In these experiments, it is the glass surface that is in contact with an electrode held at ground potential with the voltage (+1,000 or −1,000 V) applied to the cell using a tabbing wire (Figures 1–3). For the discharge from a positive bias cell, there is initially some charge at the glass to polymer interface and at the AR coating to polymer interface, Q_P. The leakage current pathway from the glass/polymer interface has the least resistance providing a negative current. Similarly, the charge at the AR coating to polymer interface, Q_{AR}, is also flowing out through the metallization but in this case contributes as a positive current because of the instrument configuration. The instrument holds the glass interface at ground and is thus actually measuring the difference between the current flow to the two electrodes, which indicates that the current flow through the glass dominates in this case. If the charge on the glass to polymer interface diminishes more quickly, then this could result in the eventual domination of the leakage current through the cell metallization producing an apparent reversal of the measured dissipation current. The electrometer is not measuring the gross outflow of current but the relative current flow out of both electrodes when the other one is held at ground. This can be thought of as measuring the current differential.

The capacitance of the AR coating is much greater than the capacitance across either the glass or the polymer layers (Table 3) and could thus initially hold much more charge. But the charge it holds is related to the resistance of the leakage pathway during charging. In the voltage off state, Equation (6) still applies, and Q_G and Q_C are negative, and Q_{AR} and Q_P are positive. The resistances to charge flow from the polymer/glass interface and the AR coating/polymer interface are empirically defined as R_{QP} and R_{QAR}, which when used in conjunction with the voltages on the opposite sides of the layers allows the calculation of the measured current ($I_{measured}$) as

$$I_{measured} = \frac{R_{QAR}C_{AR}}{2}(-Q_C + Q_{AR} + Q_P + Q_G) - \frac{R_{Qp}C_g}{2}(-Q_C - Q_{AR} - Q_P + Q_G),\quad (11)$$

which can be simplified using Equation (4) to

$$I_{measured} = R_{QAR}C_{AR}Q_C - R_{Qp}C_gQ_G.\quad (12)$$

The form looks like this because Equation (4) must still hold, but here, there is a negative residual charge most likely on both the cell and on the glass surface electrodes, which counter balances the charge within the cell layers. The capacitances do not change in time, but if Q_P dissipates at a relatively faster rate than Q_{AR}, supplying charge primarily to Q_C and Q_G, respectively, the current measured by the electrometer could invert as shown in Figure 9.

If the relative magnitudes of the resistance pathways changed, this could also create this switching of the sign of the current flow. Because the resistance through the glass is small, Q_P dissipates quickly and actually switches sign from positive to negative because the charge on the AR coating Q_{AR} is pulling negative charge from the glass making Q_G and Q_P be of the same negative sign, opposite to Q_{AR}. If subsequent to this, the resistance through the polymer became high, Q_P could eventually dissipate this negative charge as Q_{AR} approached a fully discharged state. However, because the glass is always of lower relative resistivity, it is not likely that Q_P could be discharging last. But it is possible that electrochemical potential effects could still be active here and that there could be a lot of stored charge associated with this. This is a more unusual explanation for the current reversal but could be elucidated by separately measuring the charge on both electrodes relative to ground as opposed to grounding one electrode.

This current reversal behavior was most frequently seen with the cell in positive bias but was also seen with the cell in negative bias. The repeatability of the effect shown in Figure 9 indicates that the discharge processes do not necessarily have a strong degradation effect. These two observations support the idea that there is not likely to be the effect of specific chemical reactions but more likely attributable to the distribution of charge carriers with a preference for carriers of a specific polarity and type.

To determine the underlying physics of this current reversal, we would need a better model for the current flow. This paper has outlined many different modifications to the model that could be used to predict the current flow and explain the behavior. However, these modifications add too many empirical fitting parameters, providing no confidence that the chosen model would actually explain the data. Therefore, more experiments to directly measure the different parameters are needed to better elucidate the nature of leakage current and associated electrochemical corrosion in PV modules.

4 | CONCLUSIONS

In these experiments, we created single cell test specimens to analyze the behavior of the leakage current during charging and discharging to help elucidate the nature and consequences of degradation and electrochemical corrosion effects in PV modules. We show how the early morning transient behavior in deployed modules is highly dependent on the surface conductivity, which serves to affect the amount of area for which significant current can pass. Then, the low conductivity of the glass governs the short term (~0.5 min) charging at the polymer to glass interface. The charging/discharging of this interface cannot be simply explained as a simple RC circuit. Because the capacitance of a cell is unchanged by the movement of minute amounts of charges, it must be the resistance of the glass and electrochemical potentials that are causing large deviations from simple circuit behavior. During charging, the resistance of the glass increases. Glass has too many charge carriers in it to form a space charge region throughout the

material, but we believe the depletion of thin layers of charge carriers at the surfaces can serve to increase the apparent resistivity and also produce an electrochemical potential gradient in the glass. Then, when the voltage is removed, this electrochemical gradient is hypothesized to facilitate discharge at a faster rate than during charging indicating that it, for at least short times, overrides the effect of resistance in charge depleted surface areas.

Following the initial charging upon application of voltage, there are charging effects adding minute amounts of charge to the glass/polymer interface, but the primary area of interest is the charge build-up at the AR coating to polymer interface. The charging processes at these two interfaces are active at time scales of greater than the 12 h time of these experiments. The charge does flow to a small degree through the AR coating, but in the FC cells, the overall flow is mostly to the gridlines for FC cells. However, considering that charging effects are not that much more significant for the SunPower BC cells, there must be some resistance to the electrochemical reactions at the metallization interface where the charge carriers change from ionic to electronic.

During discharge after the voltage has been removed, there is clear evidence for several different discharge processes from at least two different charge carriers within the polymer. Additionally, the discharge curve is initially too fast for the first ~0.5 min or so to be explained by linearly operating resistances. There are additional driving forces and/or complexities causing there to be an initially high driving force or alternatively a low resistance for charge transfer. We believe this is explained in part by the presence of electrochemical driving forces and/or the ability of electrochemical degradation processes to circumvent the need for ionic charge carriers to traverse the polymer to dissipate charge.

In our experiments, we measured an apparent reversal of the direction of current flow. We attribute this to electronic equipment used, which is holding one electrode at ground and measuring the relative current flow to ground. It is possible that after the removal of a positive voltage that charge in other layers could pull in negative charges to the glass/polymer interface, which could then dissipate later as a negative current, but this would require there to be some large increases in the apparent resistivity of the polymer layer, which is less likely. Therefore, we believe this current reversal phenomena to be a result of a measurement interpretation.

This work provides a framework for considering the flow of charge carriers through a photovoltaic cell or module. Current flow is very complicated having both electrostatic and chemical potential driving forces operating interactively in complicated way. Many leakage current models out there make the simplifying assumption that resistance is constant, but this work demonstrates that this is actually a bad assumption, which explains why we do not have good comprehensive leakage current models for PV and why a good understanding of the specific electrochemical processes is so elusive.

DATA AVAILABILITY STATEMENT

The data that support the findings of this study are available from the corresponding author upon reasonable request.

ORCID

Michael Kempe https://orcid.org/0000-0003-3312-0482
Peter Hacke https://orcid.org/0000-0003-4850-0947
Jichao Li https://orcid.org/0000-0002-8501-8394

REFERENCES

1. Kutzer M, Raykov A, Hahn H, et al. *Towards a root cause model for the potential-induced degradation in crystalline silicon photovoltaic cells and modules*. 2013.
2. Natrup FV, Bracht H, Murugavel S, Roling B. Cation diffusion and ionic conductivity in soda-lime silicate glasses, (in eng). *Phys Chem Chem Phys*. 2005;7(11):2279-2286. doi:10.1039/b502501j
3. Seddon E, Tippett EJ, Turner WES. The electrical conductivity of sodium meta-silicate-silica glasses. *J Soc Glass Technol*. 1932;16:450.
4. Naumann V, Lausch D, Hagendorf C. Sodium decoration of PID-s crystal defects after corona induced degradation of bare silicon solar cells. *Energy Procedia*. 2015;77:397-401. doi:10.1016/j.egypro.2015.07.055
5. Naumann V, Lausch D, Hähnel A, et al. Explanation of potential-induced degradation of the shunting type by Na decoration of stacking faults in Si solar cells. *Solar Energy Mater Solar Cells*. 2014;120:383-389. doi:10.1016/j.solmat.2013.06.015
6. Luo W, Khoo YS, Hacke P, et al. Potential-induced degradation in photovoltaic modules: a critical review. *Energ Environ Sci*. 2017;10(1):43-68. doi:10.1039/C6EE02271E
7. Berghold JD, Koch S, Frohmann B, Hacke P, Grunow P. Properties of encapsulation materials and their relevance for recent field failures. 2014 IEEE 40th Photovoltaic Specialist Conference (PVSC); 2014:1987-1992.
8. Hacke P, Glick S, Pankow J, Kempe M, Bennett SKI, Kloos M. System voltage potential-induced degradation mechanisms in PV modules and methods for test. In: *Photovoltaic Specialists Conference (PVSC), 2011 37th IEEE, 19–24 June 2011*. IEEE; 2011:814-820. doi:10.1109/pvsc.2011.6186079
9. Li J, Shen Y-C, Hacke P, Kempe M. Electrochemical mechanisms of leakage-current-enhanced delamination and corrosion in Si photovoltaic modules. *Solar Energy Mater Solar Cells*. 2018;188:273-279. doi:10.1016/j.solmat.2018.09.010
10. Kempe MD, Hacke P, Li J, Han K, Shen Y, Westerberg S. Using module leakage current modeling to understand corrosion chemistry, in 2018 IEEE 7th World Conference on Photovoltaic Energy Conversion (WCPEC) (A Joint Conference of 45th IEEE PVSC, 28th PVSEC & 34th EU PVSEC), 10–15 June 2018. 2018:3558-3563. doi:10.1109/PVSC.2018.8547741.
11. Mon GR, Ross RG, Electrochemical degradation of amorphous-silicon photovoltaic modules, in Proceedings of the 18th IEEE PV Specialists Conference, Las Vegas, Nevada, USA; 1985:1142-1149.

12. Mon GR. Electrochemical aging effects in photovoltaic modules, January 01, 1986, 1986;26:629. [Online]. Available: ui.adsabs.harvard.edu/abs/1986prin.meet..629M.

13. Warfield RW, Petree MC. Electrical resistivity of polymers. *SPE Trans*. 1961;1(2):80-85. doi:10.1002/pen.760010208

14. Cueto JAD, Rummel SR. Degradation of photovoltaic modules under high voltage stress in the field. *Proc SPIE*. 2010;7773:77730J-1–77730J-11. doi:10.1117/12.861226

15. Habersberger BM, Hacke P. *Illumination and Encapsulant Resistivity Are Critical Factors in Polarization-Type Potential Induced Degradation on n-Pert Cells*. EUPVSEC, September 2020:2020.

16. Habersberger BM, Hacke P, Madenjian LS. Evaluation of the PID-s susceptibility of modules encapsulated in materials of varying resistivity, in 2018 IEEE 7th World Conference on Photovoltaic Energy Conversion (WCPEC) (A Joint Conference of 45th IEEE PVSC, 28th PVSEC & 34th EU PVSEC), 10–15 June 2018. 2018;3807-3809. doi:10.1109/PVSC.2018.8548117

17. Reid CG, Ferrigan S, Fidalgo I, Woods JT. Contribution of PV encapsulant composition to reduction of potential induced degradation (PID) of crystalline silicon PV cells, 28th European Photovoltaic Solar Energy Conference and Exhibition, 2013.

18. Naumann V, Ilse KK, Pander M, Tröndle J, Sporleder K, Hagendorf C. Influence of soiling and moisture ingress on long term PID susceptibility of photovoltaic modules, 15th International Conference on Concentrator Photovoltaic Systems (CPV-15), 2019.

19. Li J, Han K, Shen Y-C, Westerberg S, Kempe MD, Hacke PL, Using module leakage current modeling to understand corrosion chemistry (Conference: Presented at the 2018 IEEE 7th World Conference on Photovoltaic Energy Conversion (WCPEC), 10-15 June 2018, Waikoloa Village, Hawaii). Piscataway, NJ: Institute of Electrical and Electronics Engineers (IEEE); National Renewable Energy Lab. (NREL), Golden, CO (United States), p. Medium: X. 2018.

20. Daire A. *Improving the Repeatability of Ultra-High Resistance and Resistivity Measurements*. Keithley Instruments, Inc., Instruments Business Unit.

21. Adan O, Huinink H, Reuvers NJW, Fischer H. Plasticization of nylon-6 by water: a NMR imaging study. 2013.

22. Kempe MD, Wohlgemuth JH. Evaluation of temperature and humidity on PV module component degradation, in *39th IEEE PVSC*. Tampa, Florida; 2013.

23. Hacke P, Johnston S, Luo W, Spataru S, Smith R, Repins I. Prediction of potential-induced degradation rate of thin-film modules in the field based on Coulombs transferred, in 2018 IEEE 7th World Conference on Photovoltaic Energy Conversion (WCPEC) (A Joint Conference of 45th IEEE PVSC, 28th PVSEC & 34th EU PVSEC), 10–15 June 2018. 2018;3801-3806. doi:10.1109/PVSC.2018.8547480

24. Owen-Bellini M, Hacke P, Spataru S, Miller D, Kempe M. Combined-accelerated stress testing for advanced reliability assessment of photovoltaic modules. 2018.

25. Jin X, Bai Q, Yang J, et al. Theoretical insight into leakage current of solar module under high system voltage, in 2020 47th IEEE Photovoltaic Specialists Conference (PVSC), 15 June-21 Aug. 2020. 2020; 0109–0112. doi:10.1109/PVSC45281.2020.9300364

26. Swanson R, Cudzinovic M, DeCeuster D, et al. The surface polarization effect in high-efficiency silicon solar cells, Proceedings 15th

International Photovoltaic Science and Engineering Conference (PVSEC-15), Shanghai, China; 2005:2005.

27. Lausch D, Naumann V, Graff A, et al. Sodium outdiffusion from stacking faults as root cause for the recovery process of potential-induced degradation (PID). *Energy Procedia*. 2014;55:486-493. doi:10.1016/j.egypro.2014.08.013

28. Nagel H, Metz A, Wangemann K. Crystalline Si solar cells and modules featuring excellent stability against potential-induced degradation; 2011:3107-3112.

29. Mon GR, Orehotsky J, Ross RG Jr, Whitla G. *Predicting Electrochemical Breakdown in Terrestrial Photovoltaic Modules*. Kissimmee, FL: IEEE; 1984:682-692. [Online]. Available: <Go to ISI>://INSPEC:2595632.

30. Sinha A, Moffitt SL, Hurst K, et al. Understanding interfacial chemistry of positive bias high-voltage degradation in photovoltaic modules. *Solar Energy Mater Solar Cells*. 2021;223:110959. doi:10.1016/j.solmat.2021.110959

31. Hacke P, Smith R, Terwilliger K, Glick S, Jordan D, Johnston S. Testing and analysis for lifetime prediction of crystalline silicon PV modules undergoing degradation by system voltage stress. In: *Photovoltaic specialists conference (PVSC), 2012 38th IEEE, 3–8 June 2012*; 2012: 1750-1755. doi:10.1109/pvsc.2012.6317933

32. Hacke P, Terwilliger K, Glick S, et al., Test-to-failure of crystalline silicon modules, in 2010 35th IEEE Photovoltaic Specialists Conference, 20–25 June 2010. 2010;244-250. doi:10.1109/PVSC.2010.5614472

33. Cueto J, Rummel S, Degradation of photovoltaic modules under high voltage stress in the field: preprint, Proceedings of SPIE - The International Society for Optical Engineering, vol. 7773, 08/01 2010. doi:10.1117/12.861226.

34. del Cueto JA, McMahon TJ. Analysis of leakage currents in photovoltaic modules under high-voltage bias in the field. *Progr Photovoltaics: Res Appl*. 2002;10(1):15-28. doi:10.1002/pip.401

35. Hacke P, Smith R, Kurtz S, Jordan D, Wohlgemuth J. *Modeling Current Transfer from PV Modules Based on Meterological Data*. Portland, OR: IEEE PVSC; 2016.

36. Bartczak WM, Kroh J. Theoretical models for electron conduction in polymer systems—I. Macroscopic calculations of d.c. transient conductivity after pulse irradiation. *Int J Radiat Applic Instrument Part C Radiat Phys Chem*. 1992;40(5):369-376. doi:10.1016/1359-0197(92)90197-N

37. Saidi-Amroun N, Berdous S, Saidi M, Bendaoud M. Modeling of transient currents in polyethylene terephtalate. *Int J Polym Anal Charact*. 2007;12(5):359-371. doi:10.1080/10236660701485019